Available online at www.sciencedirect.com

SciVerse ScienceDirect

journal homepage: www.elsevier.com/locate/he

Hydrogen-induced microstructural changes of Pd films

J. Čížek [a,*], O. Melikhova [a], M. Vlček [a], F. Lukáč [a], M. Vlach [a], I. Procházka [a], W. Anwand [b], G. Brauer [b], A. Mücklich [c], S. Wagner [d], H. Uchida [d], A. Pundt [d]

[a] Department of Low-Temperature Physics, Faculty of Mathematics and Physics, Charles University in Prague, V Holešovičkách 2, CZ-180 00 Praha 8, Czech Republic
[b] Institut für Strahlenphysik, Helmholtz-Zentrum Dresden-Rossendorf, Postfach 510119, D-01314 Dresden, Germany
[c] Institut für Ionenstrahlphysik und Materialforschung, Helmholtz-Zentrum Dresden-Rossendorf, PO Box 510 119, D-01314 Dresden, Germany
[d] Institut fur Materialphysik, Universität Göttingen, Friedrich-Hund-Platz 1, D-37077 Göttingen, Germany

ARTICLE INFO

Article history:
Received 18 February 2013
Accepted 18 March 2013
Available online 13 April 2013

Keywords:
Palladium films
Hydrogen
Positron annihilation spectroscopy
X-ray diffraction

ABSTRACT

The development of the microstructure in nanocrystalline, polycrystalline and epitaxial Pd films loaded with hydrogen is investigated. Structural changes in Pd films loaded with hydrogen were characterized by positron annihilation spectroscopy combined with electron microscopy and X-ray diffraction. It was found that hydrogen charging causes plastic deformation which leads to an increase of the defect density in all Pd films studied. Moreover, the formation of buckles was observed in nanocrystalline and polycrystalline Pd films loaded above a certain critical hydrogen concentration. Buckling leads to detachment of the film from the substrate and this is accompanied with in-plane stress relaxation and plastic deformation of the film.

1. Introduction

Hydrogen dissolved in interstitial sites in a host metal lattice causes remarkable volume expansion. On the one hand, bulk samples loaded with hydrogen expand in all directions and the lattice expansion increases with increasing hydrogen concentration. On the other hand, thin films are usually deposited on a stiff substrate which hinders in-plane expansion of the film. This makes expansion of the film loaded with hydrogen strongly anisotropic: the in-plane expansion is suppressed, while the out-of-plane expansion is remarkably larger than in a free-standing bulk metal. As a consequence, high compressive bi-axial in-plane stresses up to several GPa occur in thin films loaded with hydrogen [1,2]. These hydrogen-induced stresses grow with increasing hydrogen content and may cause local or global detachment of the loaded film from the substrate resulting in formation of buckles with various morphologies [3–5]. Hence, the behaviour of hydrogen-loaded thin films fixed on substrates is quite different from that of corresponding bulk samples [6,7] since thin films are strongly influenced by stress imposed to the virgin film by its adhesion to a substrate, hydrogen-induced bi-axial stresses, and the film microstructure itself [1,8,9]. Understanding and prediction of hydrogen behaviour in thin films and hydrogen-induced buckling is highly important since this process may cause catastrophic adhesion failure in many thin film systems or coatings exposed to hydrogen.

* *Corresponding author*. Tel.: +420 2 21912788; fax: +420 2 2191 2567.
E-mail address: jakub.cizek@mff.cuni.cz (J. Čížek).
0360-3199/$ – see front matter
http://dx.doi.org/10.1016/j.ijhydene.2013.03.096

Pd is often used as a model system for the investigation of hydrogen in a metal lattice since Pd can absorb a relatively large amount of hydrogen and it can be easily charged with hydrogen [10]. Moreover, Pd films are widely used in hydrogen technologies due to a high mobility of hydrogen in the Pd lattice [10] and a catalytic effect of thin Pd layer on hydrogenation of a variety of materials [11–13]. Pd films are used also as the gate electrodes of metal-oxide-semiconductor hydrogen sensors [14].

In the present work we used Pd films as a model system for the investigation of structural changes caused by absorbed hydrogen. Nanocrystalline, polycrystalline and epitaxial Pd films were prepared and charged with hydrogen in order to examine the effect of microstructure on the behaviour of absorbed hydrogen. Variable energy slow positron implantation spectroscopy (VEPAS) [15] was employed as a principal technique for characterization of defects in Pd films. VEPAS is a non-destructive technique which provides depth sensitive information about open-volume defects, e.g. vacancies, dislocations, open volumes at grain boundaries etc. In the present work VEPAS was combined with structural investigations by synchrotron radiation X-ray diffraction (XRD) and electron microscopies.

2. Experimental details

Thin Pd films were deposited on polished (11–20) sapphire substrates by cold cathode beam sputtering in a UHV chamber (10^{-10} mbar) using a Pd target with purity of 99.95%. Three kinds of samples have been prepared: (i) *nanocrystalline films* deposited at room temperature; (ii) *polycrystalline films* deposited at room temperature and then annealed in the UHV chamber at a temperature of 800 °C for 1 h; (iii) *epitaxial films* deposited at a temperature of 800 °C. The thickness of the deposited films was determined by stylus profilometry. Nanocrystalline films with two different thicknesses (490 ± 5 nm and 1080 ± 10 nm) were prepared in order to examine a possible influence of the film thickness on hydrogen absorption. The thickness of a polycrystalline and epitaxial film was (1040 ± 10) nm and (485 ± 5) nm, respectively.

The samples were then step-by-step doped with hydrogen by electrochemical charging [12] in a galvanic cell filled with a 1:2 mixture of H_3PO_4 and glycerine. The charging was performed by constant current pulses between a Pt counter electrode (anode) and the loaded sample (cathode). The current density on the sample was 0.1 mA/cm^2. The hydrogen concentration in the loaded sample was calculated from the transported charge using Faraday's Law and is expressed as the atomic ratio H/Pd throughout this paper. A bulk Pd sample (99.95%) supplied by MaTecK GmbH and annealed at 1000 °C for 1 h in vacuum was used as a reference sample.

VEPAS studies were performed on a magnetically guided positron beam SPONSOR [16] with positron energy adjustable from 0.03 to 36 keV. Doppler broadening of the annihilation line was evaluated using the line shape parameters S and W [15].

The S-parameter is calculated as ratio of a suitably selected central area of the annihilation peak (centred at 511 keV) to the net peak area [15]. Usually the central region is selected so that the S-parameter value of a defect-free reference is close to 0.5. In the present work the energy interval was (510.54, 511.46) keV. This choice leads to the value $S_0 = 0.4968(7)$ for a well-annealed reference bulk Pd sample at a positron energy $E = 36$ keV. All S parameters reported in this work are normalized to the S_0 value.

The W-parameter is a ratio of the wing areas of the annihilation peak selected here as 504.00–507.43 keV and 514.57–518.00 keV to the net peak area. All W-parameters reported in this work were normalized to the value $W_0 = 0.0977(3)$ obtained for a well-annealed reference bulk Pd sample at a positron energy $E = 36$ keV.

Narrowing of the annihilation peak (i.e. smaller Doppler shift) leads to an increase of the S-parameter and a decrease of the W-parameter. Localization of a positron in an open-volume defect causes a reduction of positron annihilations with high momentum core electrons. As a consequence, the annihilation peak becomes narrower and the S-parameter increases while the W-parameter decreases. Thus, S-parameter is a measure of the density of open-volume defects in the specimen, in case that type of defects remains unchanged.

Fitting of the dependence of the S-parameter on positron energy was performed by the VEPFIT software package [17], which solves the positron diffusion-annihilation equation in a single-layer model (Pd film) for films with a thickness of $\approx$1000 nm or a two-layer model (Pd film + substrate) for films with smaller thickness.

XRD studies of Pd films were carried out using synchrotron radiation with wavelength of $\lambda = 0.499$ Å in HASYLAB (DESY, Beamline B2) at a beamline equipped with a four-axis Eulerian cradle. The XRD measurements were performed in the Bragg–-Brentano symmetrical geometry and the XRD profiles were fitted by the Pearson VII function. The out-of-plane lattice parameters of Pd films were determined from the positions of (111) and (222) Pd reflections using the Cohen–Wagner extrapolation plot. Texture measurements were performed on X'Pert MRD powder diffractometer (PANalytical B.V.) equipped with a polycapillary and Eulerian cradle using Co K_α radiation (wavelength 1.788965 Å).

Transmission electron microscopy (TEM) was carried out using a Philips CM300SuperTWIN microscope operating at 300 kV. Thin foils for cross-sectional TEM were produced by conventional preparation using Gatan precision ion polishing system (PIPS). Morphology of Pd films was examined also by scanning electron microscopy (SEM) using scanning electron microscope JEOL JSM-7500F. A metallographic light microscope Arsenal AM-2T was used for observations of buckling in hydrogen-loaded films.

3. Results and discussion

3.1. Structure of virgin films

3.1.1. Nanocrystalline films

Fig. 1 shows a cross-sectional TEM micrograph of a virgin Pd film with thickness of 1080 nm deposited at room temperature. The SEM image of the surface of the Pd film is shown in Fig. 2a. From an inspection of the figures one can conclude that the film exhibits nanocrystalline column-like grains having a width of ~50 nm. On TEM images one can distinguish two kinds of columns: (i) 'first generation columns' with average height of ~200 nm growing directly on the sapphire surface and (ii) 'second generation columns' growing on the

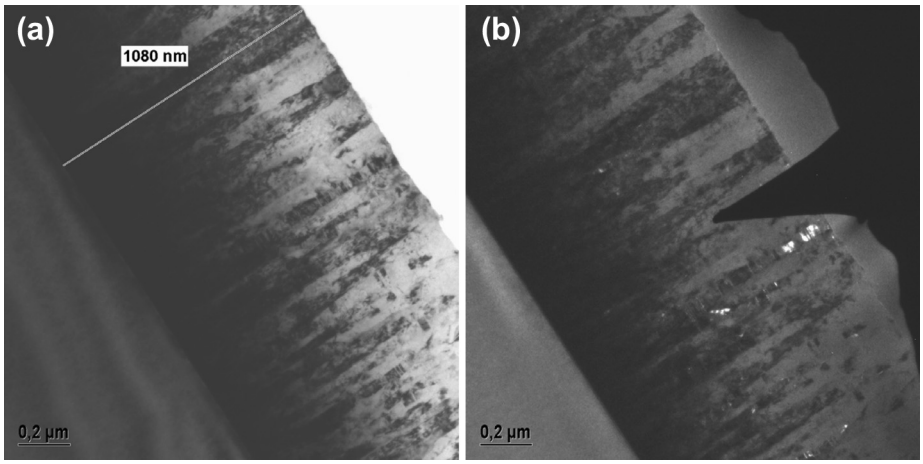

Fig. 1 – TEM micrographs of a cross-section of a virgin nanocrystalline Pd film with a thickness of 1080 nm (a) bright field image, (b) dark-field image.

top of the first generation. A very similar microstructure was observed also on thinner Pd film with thickness of 490 nm deposited at room temperature (not shown here). A similar kind of structure consisting of two generations of columnar crystallites was found also in nanocrystalline Nb films [18].

The XRD pattern measured on the nanocrystalline Pd film in the symmetrical Bragg–Brentano geometry exhibits (111) and (222) Pd reflections and a sharp (2–10) reflection from the sapphire substrate. The profile of the (111) Pd reflection measured in the nanocrystalline film with a thickness of 1080 nm is plotted in Fig. 3a. An asymmetrical shape of the (111) Pd reflection indicates that it is actually a superposition of two contributions originating from the first- and second-generation crystallites. These two contributions were considered in fitting of the reflection and are plotted in Fig. 3a by dashed lines. The (111) Pd reflections for both generations of crystallites are located at lower diffraction angles than the position for a perfect Pd crystal indicated in Fig. 3a by a vertical dashed line. This testifies to compressive in-plane stress in the virgin film caused by a lattice mismatch between the Pd layer and the sapphire substrate. The Pd film is compressed in the plane of the substrate in order to match better the interatomic distance in the sapphire substrate and to reduce the interfacial energy between the film and the substrate. Compression of the film in the plane of the substrate by a compressive bi-axial in-plane stress simultaneously causes its expansion in the perpendicular out-of-plane direction. Hence, the lattice parameter in the out-of-plane direction, which is measured in the symmetrical Bragg–Brentano geometry, is expanded compared to that of a bulk Pd crystal. The highest compressive stress occurs close to the interface with the sapphire substrate, i.e. in the first generation columns, where the film is squeezed most of all. With increasing distance from the substrate the compressive stress decreases, the compression of the film is more and more relaxed and the lattice parameter approaches the value for a free-standing bulk Pd crystal. The out-of-plane lattice parameters determined for both generations of crystallites are plotted in Fig. 4.

A pole figure for the (200) Pd reflection measured in the nanocrystalline Pd film with a thickness of 1080 nm is plotted

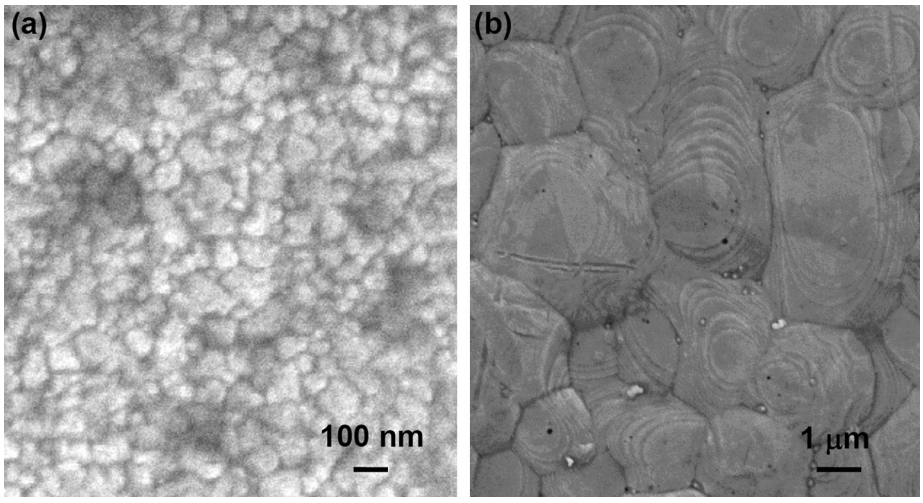

Fig. 2 – SEM micrographs of virgin Pd films (a) nanocrystalline film deposited at room temperature, (b) polycrystalline film deposited at room temperature and annealed at 800 °C for 1 h.

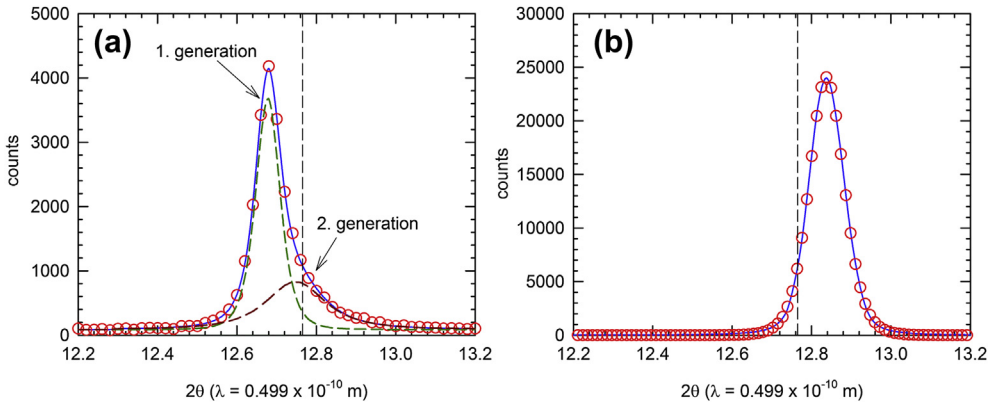

Fig. 3 – Profile of the (111) Pd reflection measured by XRD on virgin Pd films (a) nanocrystalline film deposited at room temperature, (b) polycrystalline film deposited at room temperature and annealed at 800 °C for 1 h. The solid lines show a fit of the reflections by a Pearson VII model function. In case of the nanocrystalline film (left panel) the model function consists of a contribution of the first and the second generation crystallites shown by dashed lines. The position of the (111) Pd reflection in a perfect Pd crystal is indicated by a vertical dashed line.

in Fig. 5a. Nanocrystalline Pd films exhibit (111) fibre texture, i.e. most of crystallites grow so that {111} Pd planes are parallel with the substrate but the lateral orientation of the crystallites in the plane of substrate is completely random.

3.1.2. *Polycrystalline films*

Fig. 2b shows a SEM image of a Pd film deposited at room temperature and then annealed at 800 °C for 1 h. One can see in the figure that annealing at 800 °C led to a significant grain growth of original nanocrystalline grains resulting in a polycrystalline structure with the mean lateral grain size of ~2.5 μm. Recrystallization took place in the whole Pd film and wiped out differences between the first and the second-generation crystallites. Indeed, Fig. 3b shows that the (111) Pd reflection measured on the polycrystalline film is symmetrical and can be well described by a single contribution. The position of (111) Pd reflection is located at higher diffraction angles than the position for a perfect Pd crystal indicated by a vertical dashed line. Hence, contrary to nanocrystalline films, a polycrystalline film suffers from tensile in-plane stress and the out-of-plane lattice constant in the polycrystalline film is lower than in bulk Pd, see Fig. 4. The tensile in-plane stress is caused by different thermal expansion of the Pd layer and the sapphire substrate. During annealing at elevated temperature when recrystallization takes place, Pd atoms are arranged into configuration with higher inter-atomic spacing corresponding to the elevated temperature. Since the thermal expansion of the sapphire substrate [19] is lower than that of Pd [20], shrinkage of the Pd lattice during cooling of the film from elevated temperatures is hindered by the substrate leading finally to residual tensile stress in the film at room temperature.

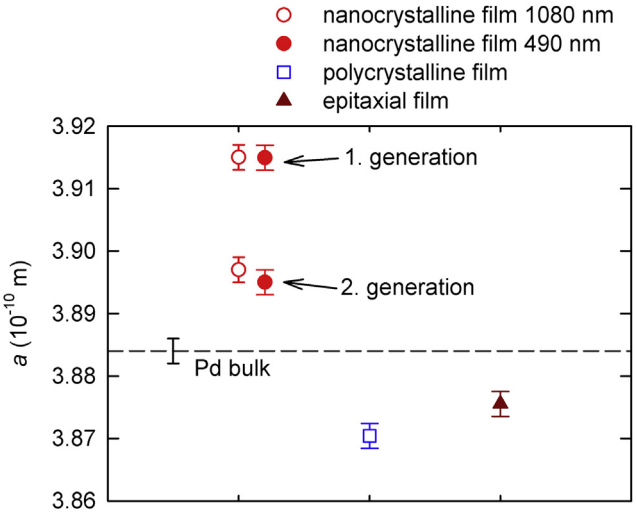

Fig. 4 – The out-of-plane lattice parameters determined in virgin Pd films by XRD. The dashed line shows the lattice parameter for a perfect Pd crystal.

A pole figure for the (200) Pd reflection plotted in Fig. 5b shows a development of texture caused by annealing at 800 °C. In a polycrystalline film most of grains grow with {111} planes parallel with the substrate, but contrary to nanocrystalline films, the lateral orientation of grains is not random and one orientation in the plane of the substrate is preferred.

3.1.3. *Epitaxial films*

A pole figure for the (200) Pd reflection shown in Fig. 5c testifies that an epitaxial film exhibits a single orientation with respect to the substrate. A sharp texture of the epitaxial film is demonstrated also by an ω-scan for the (111) Pd reflection plotted in Fig. 6a. Obviously the epitaxial film exhibits a substantially narrower peak compared to the nanocrystalline film.

The profile of the (111) Pd reflection measured by XRD in the epitaxial Pd film is plotted in Fig. 6b. The width of the (111) Pd reflection in the epitaxial film is narrower than in other films studied and has a symmetrical shape which can be well described by a single contribution. The position of the (111) Pd reflection is shifted to higher diffraction angles with respect to the position for a perfect Pd crystal indicated in Fig. 6b by a vertical dashed line. Hence, the epitaxial Pd film exhibits an out-of-plane lattice parameter lower than in bulk Pd, see

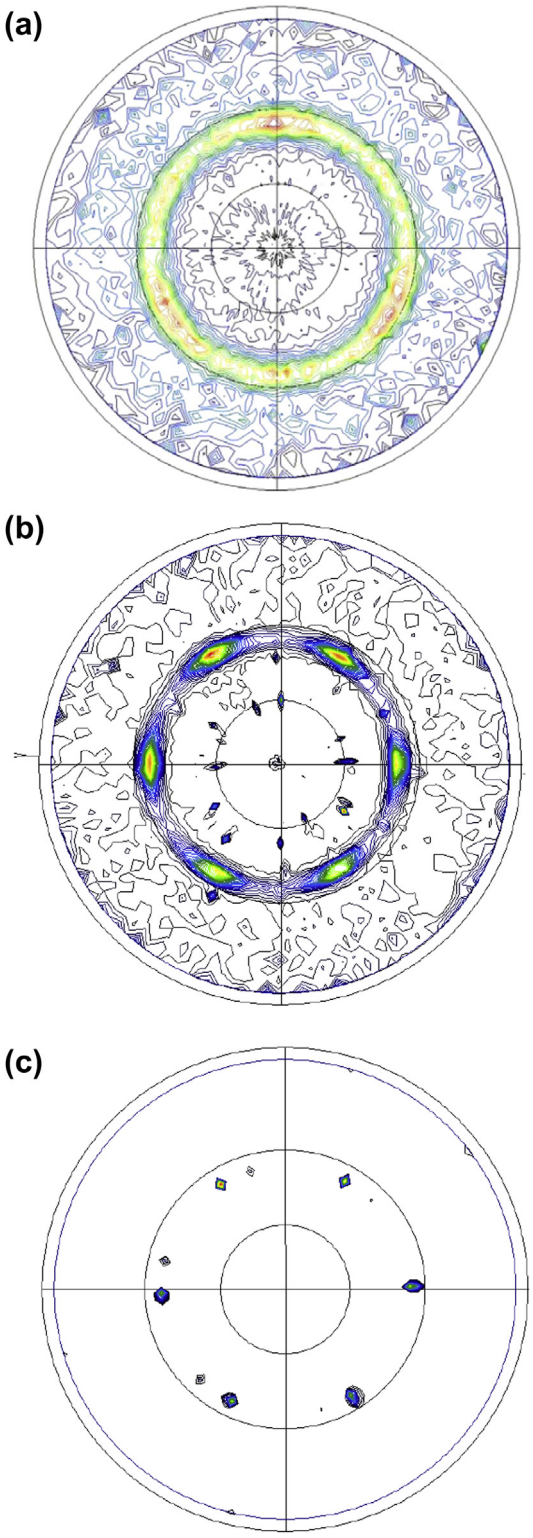

Fig. 5 – Pole figures for the (200) Pd reflection measured on virgin Pd films (a) nanocrystalline film, (b) polycrystalline film, (c) epitaxial film.

Fig. 4. Similarly to the polycrystalline film, also the epitaxial film suffers from in-plane tensile stress caused by the difference of the thermal expansion coefficient in Pd layer and sapphire substrate.

3.2. *Defects in virgin films*

Results of VEPAS investigations of virgin samples are presented in Fig. 7. The dependence of the S-parameter on the positron energy E for virgin Pd films (nanocrystalline film with thickness of 1080 nm, polycrystalline film and epitaxial film) are plotted in Fig. 7a. The $S(E)$ curve for the reference well-annealed bulk Pd sample is plotted in the figure as well. At very low energies virtually all positrons annihilate on the surface. With increasing energy positrons penetrate deeper and deeper into the sample and the fraction of positrons diffusing back to the surface decreases. This is reflected by a gradual decrease of the S-parameter from the surface value S_{surf} down to the bulk value S_0 corresponding to the situation when all positrons annihilate inside bulk Pd. The dependence of the S-parameter on positron energy for the reference bulk Pd sample was fitted by a model function calculated by the VEPFIT software [17] as a solution of the positron diffusion-annihilation equation in a single-layer structure. One can see in Fig. 7a that the model function plotted in the figure by a solid line describes experimental points accurately. The mean positron diffusion length $L_{+,B} = (151 \pm 4)$ nm was obtained for the reference well-annealed bulk Pd from fitting. This value is comparable with the positron diffusion length in metals with a very low concentration of defects [15]. Positron lifetime studies of the well-annealed bulk Pd sample revealed a single component spectrum with a lifetime $\tau_B = (112 \pm 4)$ ps which agrees well with the bulk positron lifetime in Pd obtained from *ab-initio* theoretical calculations [21]. Hence, the well-annealed reference bulk Pd sample can be considered as a defect-free material since it exhibits a very low concentration of defects which falls below the sensitivity limit of positron annihilation spectroscopy.

The dependence of the S-parameter on the positron energy E in a Pd film can be described by the expression

$$S(E) = S_{surf} f_{surf}(E) + S_{Pd} f_{Pd}(E) + S_{substrate} f_{substrate}(E), \quad (1)$$

where S_{surf}, S_{Pd} and $S_{substrate}$ denote the S-parameter for positrons annihilated on the surface, in the Pd layer and in the substrate, respectively. A similar equation can be written also for the W-parameter. The symbols f_{surf}, f_{Pd} and $f_{substrate}$ stand for the fraction of positrons annihilated on the surface, in the Pd layer and in the substrate, respectively. These fractions depend on positron energy but always satisfy a normalization condition.

$$f_{surf}(E) + f_{Pd}(E) + f_{substrate}(E) = 1. \quad (2)$$

The fractions f_{surf}, f_{Pd} and $f_{substrate}$ were calculated by VEPFIT software [17] as a solution of the positron diffusion-annihilation equation in a two-layer structure consisting of (i) the Pd film and (ii) the sapphire substrate. The property of the Pd layer is characterized by its S-parameter S_{Pd} and the mean positron diffusion length $L_{+,Pd}$ in the Pd layer. These parameters were obtained by fitting of the model curve given by Eq. (1) to the experimental points.

The mean penetration depth of positrons with an energy $E = 25$ keV (i.e. the maximum energy of incident positrons used for VEPAS investigations of thin Pd films in this work) into Pd is ≈570 nm. Hence, in thinner films studied in this work having a thickness around 500 nm some fraction of

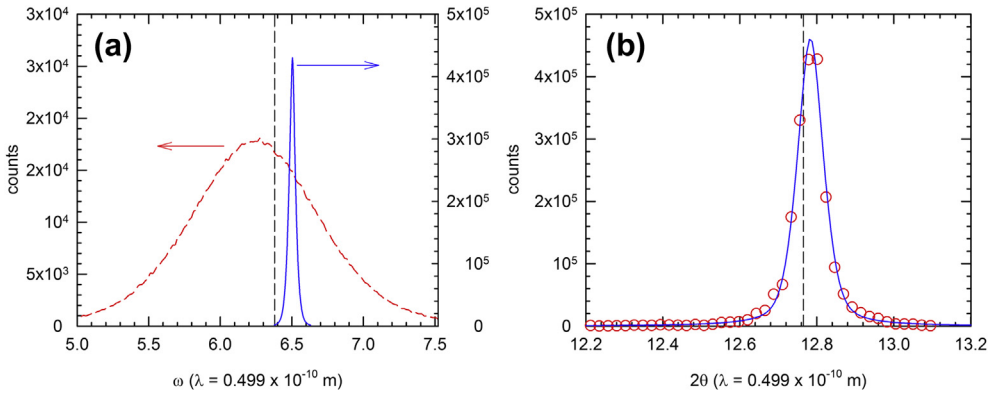

Fig. 6 – (a) ω-Scans for the (111) Pd reflection measured in a nanocrystalline Pd film (dashed line) and an epitaxial Pd film (solid line); (b) profile of the (111) Pd reflection measured in a virgin epitaxial Pd film. The solid line is a fit by a Pearson VII model function. The position of the (111) Pd reflection in a perfect Pd crystal is indicated by a vertical dashed line.

positrons definitely penetrates into the substrate when the positron energy approaches 25 keV. On the other hand, positrons implanted into thicker Pd films with a thickness around 1000 nm are not able to penetrate into the substrate, i.e. $f_{substrate}(E) = 0$.

Compared to the reference well-annealed bulk Pd sample, the nanocrystalline Pd film (thickness of 1080 nm) exhibits substantially higher S parameters, see Fig. 7a. Moreover, the mean positron diffusion length $L_{+,Pd} = (41 \pm 5)$ nm, obtained from fitting of the $S(E)$ curve for the nanocrystalline Pd film, is significantly shorter than $L_{+,B}$ in the well-annealed reference bulk Pd sample. The enhanced S-parameter and the shortened positron diffusion length give clear evidence that the nanocrystalline Pd film contains a significant density of positron traps. This is not surprising since the average width of nanocrystalline columns in the nanocrystalline Pd film (~50 nm) is comparable with the positron diffusion length. Hence, there is a high probability for positron trapping in vacancy-like open-volume defects at interfaces between crystallites.

The polycrystalline Pd film exhibits remarkably lower S-parameter and a longer positron diffusion length than the nanocrystalline film. This is caused by a significant grain growth which took place during annealing of the film resulting in a dramatic decrease of positron trapping in the vacancy-like open-volume defects at grain boundaries. The mean positron diffusion length $L_{+,Pd} = (106 \pm 1)$ nm was obtained from fitting of the $S(E)$ curve for the polycrystalline Pd film. This value is smaller than $L_{+,B}$ but significantly larger than the positron diffusion length in the nanocrystalline film. Hence, the defect density in the polycrystalline Pd film is significantly lower than in the nanocrystalline film, but higher than in the well-annealed bulk Pd reference sample.

The epitaxial Pd film exhibits the highest S-parameter among all the samples studied, see Fig. 7a. Since the thickness of the epitaxial Pd film is 485 nm only, at high energies ($E > 15$ keV) some fraction of positrons penetrates into the sapphire substrate leading to a decrease of the S-parameter. The mean positron diffusion length $L_{+,Pd} = (16 \pm 2)$ nm obtained from fitting of the $S(E)$ curve for the epitaxial film is the shortest one among all the samples studied. Hence, the epitaxial film contains the highest concentration of positron traps. It is well known that the formation of misfit dislocations is a most common mechanism for stress accommodation in epitaxial films [22] and misfit dislocations form a dense

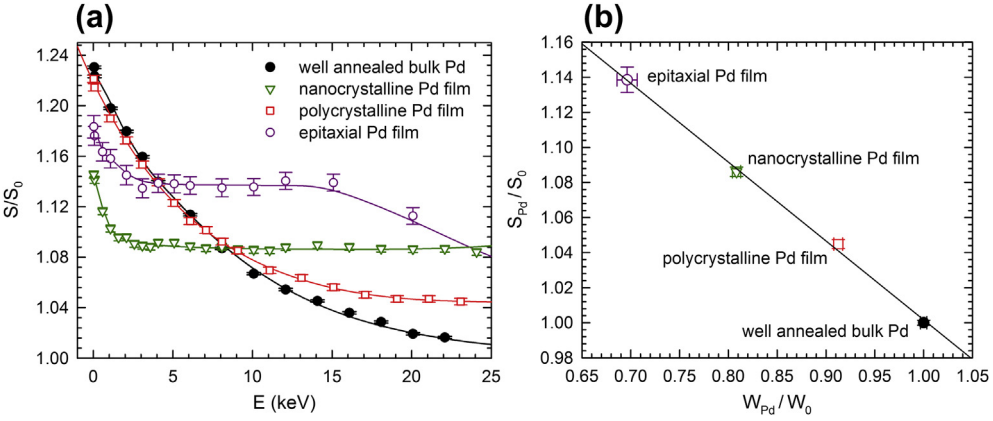

Fig. 7 – VEPAS results obtained on virgin samples: (a) dependence of the S-parameter on positron energy E for virgin films and a reference well-annealed bulk Pd sample. Solid lines show model curves calculated by the VEPFIT software; (b) S–W plot constructed from S- and W-parameters for a Pd layer obtained from fitting of experimental $S(E)$ curves.

pattern at the film-substrate interface [23]. Moreover, except of misfit dislocations located at the film-substrate interface, additional dislocations are expected to be present inside the epitaxial film due to threading dislocations extending from the substrate into the film [23]. Hence, a very high S-parameter and short positron diffusion length in the epitaxial Pd film is due to positron trapping at dislocations. The density of dislocations in the epitaxial Pd film can be estimated from the equation [24]

$$\rho_D = \frac{1}{\nu_D \tau_B}\left(\frac{L_{+,B}^2}{L_+^2} - 1\right), \quad (3)$$

where $\tau_B = 112$ ps is the bulk positron lifetime in Pd and $\nu_D \approx 0.5 \times 10^{-4}\ m^2\ s^{-1}$ [25,26] is the specific positron trapping rate to dislocations. The mean dislocation density in the epitaxial Pd film estimated by Eq. (3) is $\rho_D \approx 2 \times 10^{16}\ m^{-2}$.

It is well known that a dislocation line itself is only a shallow positron trap [25,26]. When a positron arrives at the core of a dislocation line, it diffuses quickly along the line (pipe diffusion) until it finds a vacancy attached to the dislocation and is trapped there. Hence, positron trapping at dislocations is controlled by the dislocation density, but positron confinement in the dislocation is only a transient state and positrons are finally annihilated in vacancy-like defects.

Fig. 7b shows so called S–W plot, i.e. a correlation plot of the S-parameter S_{Pd} versus the W-parameter W_{Pd} for Pd films and the reference bulk sample. Obviously all [W_{Pd}, S_{Pd}] points in Fig. 7b fall on a straight line connecting the well-annealed bulk Pd sample and the epitaxial Pd film. This testifies that all Pd films contain a similar kind of defects (i.e. vacancy-like misfit defects at grain boundaries and/or vacancies attached to misfit dislocations) and differ by concentration of these defects only.

3.3. *Hydrogen-loaded films*

Fig. 8a shows selected XRD profiles of the (111) Pd reflection for a hydrogen-loaded nanocrystalline Pd film with a thickness of 1080 nm. The (111) reflection in a hydrogen-loaded film remains asymmetric, which testifies that the difference in the inter-planar spacing in the first and the second generation crystallites remains during hydrogen loading. Fig. 9a shows the lattice parameters in the first and the second generation crystallites plotted as a function of the hydrogen concentration x_H in the nanocrystalline films. Absorbed hydrogen causes an expansion of the Pd film in the out-of-plane direction, which can be seen as a shift of the (111) Pd reflections to lower diffraction angles. An increase of the out-of-plane lattice parameter both in the first- and the second-generation crystallites can be clearly seen in Fig. 9a. At low hydrogen concentrations ($x_H \leq 0.02$) the film expansion occurs elastically, i.e. without formation of dislocations. With increasing hydrogen concentration the hydrogen-induced stresses strongly increase and when the yield stress in Pd is exceeded plastic deformation of the film takes place. Plastic deformation introduces dislocations into the film and the film structure becomes less perfect. This is reflected by a broadening and a decrease of intensity of XRD peaks in Fig. 8a. Since hydrogen-induced stress is partially released by plastic deformation, the slope of the increment of lattice parameters is lowered when plastic deformation occurs, see Fig. 9a.

High internal stresses introduced during hydrogen loading may lead to a situation when detachment of film from the substrate is energetically favourable and buckles of various shapes are formed [3,4,27]. Buckling of the film occurs at a certain critical concentration of absorbed hydrogen when the stored elastic strain energy overcomes the adhesion energy and hydrogen-induced stresses cause crack formation at the interface between the film and the substrate [3]. In the nanocrystalline Pd film buckling started at $x_H > 0.05$ by formation of straight buckles in the film. However, since a straight buckle can release the in-plane stress in a one direction only [3] it is forced to expand also in the perpendicular direction and straight buckles become curved at later stages of buckling. Eventually a complicated pattern of many buckles of undulated shape shown in Fig. 8b was formed in the film loaded up to a hydrogen concentration $x_H = 0.3$. Further hydrogen charging led to a complete detachment of the nanocrystalline film from the substrate. Hydrogen-induced buckling occurs in the same range of hydrogen concentrations in both nanocrystalline films studied.

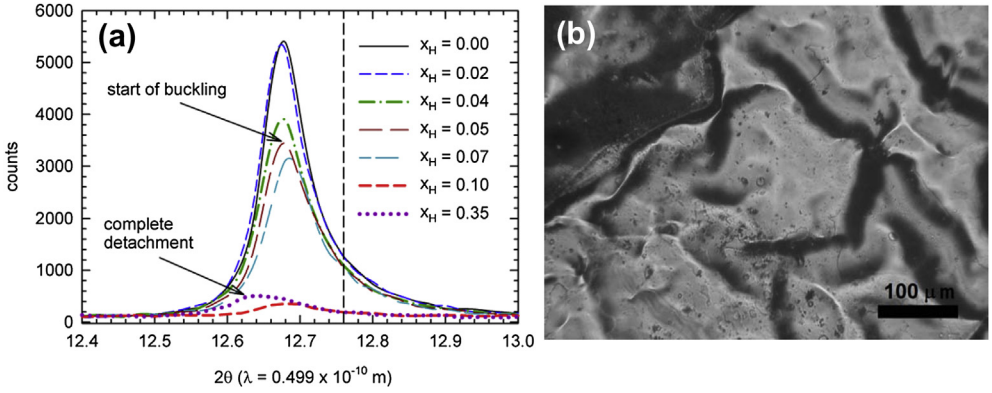

Fig. 8 – (a) Selected profiles of the (111) Pd reflection measured by XRD on the nanocrystalline Pd film (thickness of 1080 nm) charged with hydrogen up to various hydrogen concentrations x_H. The vertical dashed line indicates the position of the (111) Pd reflection in a perfect bulk Pd crystal; (b) light microscopy image of a buckled nanocrystalline Pd film loaded with hydrogen up to $x_H = 0.30$.

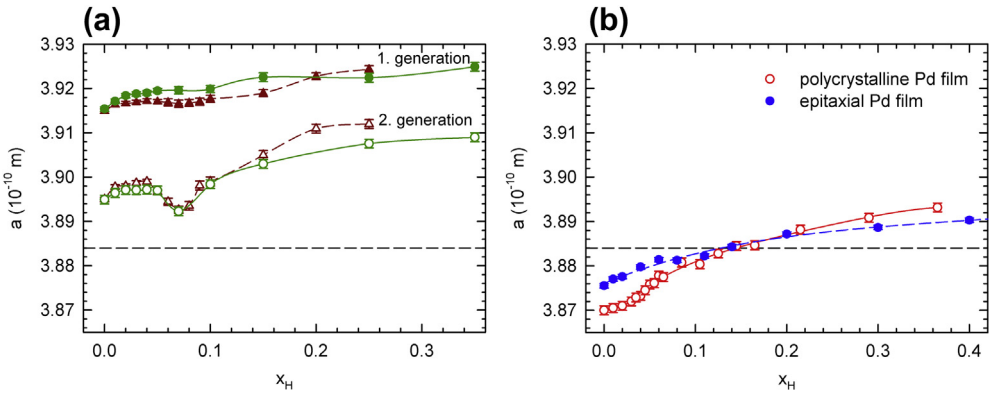

Fig. 9 – (a) Out-of-plane lattice parameter for the first (full symbols) and the second (open symbols) generation crystallites as a function of hydrogen concentration x_H in a nanocrystalline film with thickness of 1080 nm (circles) and 490 nm (triangles). (b) Dependence of the out-of-plane lattice parameter on the hydrogen concentration for a polycrystalline film (open circles) and an epitaxial film (full circles). The lattice parameters were always obtained from the Cohen–Wagner extrapolation plot using the positions of the (111) and (222) Pd reflections. The horizontal dashed line shows the lattice parameter for a perfect bulk Pd crystal.

One can see in Fig. 8a that buckling of a hydrogen-loaded film causes a strong drop of intensity of XRD reflections because of misalignment of the film surface and defocusing. Parts of the film which were detached from the substrate become free and their in-plane expansion is not suppressed by the substrate anymore. As a consequence, in-plane relaxation takes place in the detached parts of the film leading to a drop of the out-of-plane lattice constant, which can be clearly seen in Fig. 9a at a hydrogen concentration of $x_H \approx 0.07$. After the in-plane relaxation due to hydrogen-induced buckling, the lattice parameter further increases with increasing hydrogen content.

The occurrence of the α'-phase (Pd hydride) with a face centred cubic structure and lattice parameter of (4.017 ± 0.005) Å was detected in the nanocrystalline film at hydrogen concentrations $x_H \geq 0.15$. Thus, the hydrogen solubility in the α-phase in the nanocrystalline Pd film is roughly eight times higher than in a conventional bulk Pd polycrystal [28]. This effect, which was observed also in other nanocrystalline films [6,9,29], is due to the nanocrystalline structure of the Pd film, which contains a significant volume fraction of grain interfaces, able to accumulate more hydrogen than grain interiors. Moreover, high internal stresses in thin films may influence hydrogen solubility in the α-phase as well [6].

From inspection of Fig. 9a it becomes clear that the development of lattice parameters is very similar in both the nanocrystalline films, i.e. the film with thickness of 1080 nm and 490 nm. This indicates that the film thickness does not play an important role for films thicker than ≈500 nm.

Selected $S(E)$ curves for the nanocrystalline Pd film (thickness of 1080 nm) charged with hydrogen are plotted in Fig. 10a. The $S(E)$ curves were analyzed by VEPFIT and the calculated model curves are plotted in the figure by solid lines. Fig. 10b shows a dependence of the S-parameter S_{Pd} and the mean positron diffusion length $L_{+,Pd}$ for a nanocrystalline Pd layer obtained from fitting of the $S(E)$ curves on the hydrogen concentration x_H. Vacancy-like defects at grain boundaries between nanocrystalline grains act as trapping sites for hydrogen atoms [9]. At low concentrations ($x_H \leq 0.01$), hydrogen preferentially fills the open-volume defects at grain interfaces. Since positrons in the nanocrystalline film are

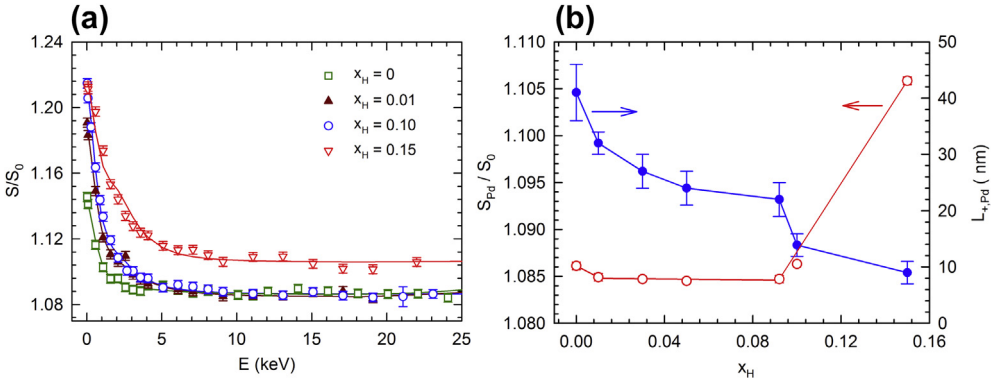

Fig. 10 – (a) Selected $S(E)$ curves for a nanocrystalline Pd film (thickness of 1080 nm) charged with hydrogen. The solid lines show the model curves calculated by the VEPFIT software; (b) S-parameter S_{Pd} and the mean positron diffusion length $L_{+,Pd}$ obtained from fitting of the $S(E)$ curves plotted as a function of hydrogen concentration x_H.

annihilated predominantly from a trapped state in defects at grain interfaces, VEPAS is sensitive to a filling of grain interfaces by hydrogen. Fig. 10b shows a decrease of S_{Pd} at low hydrogen concentration $x_H \approx 0.01$. This is caused by hydrogen trapping in vacancy-like misfit defects at grain interfaces leading to a reduced localization of the positron wave function due to a repulsive interaction between a confined positron and a hydrogen atom trapped at the defect. At higher hydrogen concentrations ($x_H > 0.01$), all available deep traps at grain boundaries are already filled by hydrogen and S_{Pd} remains approximately constant. Finally a dramatic increase of S_{Pd} accompanied by a drop of the positron diffusion length $L_{+,Pd}$ occurs at $x_H > 0.09$, i.e. at hydrogen concentrations when buckling of the film takes place. This testifies a positron trapping at new defects, presumably dislocations, introduced into the film during buckling.

The development of the out-of-plane lattice parameter in a hydrogen-loaded polycrystalline Pd film is plotted in Fig. 9b. The out-of-plane lattice parameter increases due to hydrogen-induced lattice expansion. However because of the in-plane tensile stress imposed by the substrate the out-of-plane lattice parameter of the film remains lower than that for a bulk Pd crystal up to a hydrogen concentration of $x_H \approx 0.14$. The reflections corresponding to the β-phase appeared in the XRD pattern for the polycrystalline film loaded to hydrogen concentrations $x_H > 0.14$, i.e. the phase boundary between α and β phase is shifted to a hydrogen concentration significantly higher than in a bulk Pd crystal. This is caused by tensile in-plane stress in the polycrystalline film which leads to the out-of-plane lattice parameter lower than in bulk Pd. As hydrogen absorbed in the polycrystalline film causes a lattice expansion in the out-of-plane direction, it remains in the α-phase until $x_H \approx 0.14$ when the out-of-plane lattice parameter becomes comparable with that of bulk Pd, see Fig. 9b. Buckling of the polycrystalline films was observed at hydrogen concentrations $x_H > 0.4$, i.e. at significantly higher hydrogen concentrations than in the nanocrystalline films. This indicates that annealing at 800 °C improved the bonding of the Pd film to the sapphire substrate.

The $S(E)$ curves for the polycrystalline Pd film charged with hydrogen are plotted in Fig. 11a. The S-parameter S_{Pd} and the mean positron diffusion length $L_{+,Pd}$ for the Pd layer obtained from fitting of $S(E)$ curves are plotted in Fig. 11b as a function of hydrogen concentration. Hydrogen charging leads to an increase of the concentration of defects in the polycrystalline Pd film which is reflected by a monotonic increase of S_{Pd} and simultaneous decrease of $L_{+,Pd}$. This behaviour gives clear evidence for a hydrogen-induced plastic deformation taking place in the polycrystalline film. Since the volume fraction of grain interfaces in a polycrystalline film is negligible due to a relatively large size of crystallites filling of vacancy-like misfit defects at grain boundaries by hydrogen cannot be detected in contrast to the nanocrystalline film. Moreover, a strong rise of the defect concentration associated with buckling is not seen in Fig. 11b since buckling of the polycrystalline film takes place at $x_H > 0.4$ only.

The development of the out-of-plane lattice parameter of the epitaxial Pd film loaded with hydrogen is shown in Fig. 9b. Similarly to the polycrystalline film also the virgin epitaxial film exhibits an out-of-plane lattice parameter lower than that for a bulk Pd. With increasing hydrogen concentration the epitaxial film expands in the out-of-plane direction and the out-of-plane lattice parameter increases and approaches the value for a bulk Pd crystal at a hydrogen concentration of $x_H \approx 0.14$. Similarly to the polycrystalline film β-phase is formed in the epitaxial film at hydrogen concentrations $x_H > 0.14$, when the out-of-plane lattice parameter exceeds that for a bulk Pd crystal. Since no buckling of the epitaxial film was observed in the whole range of hydrogen concentrations examined in this work (i.e. up to $x_H = 0.4$) one can conclude that the best bonding of the Pd layer to the sapphire substrate was achieved in the epitaxial film deposited at elevated temperature.

Fig. 12a shows $S(E)$ curves for the epitaxial Pd film loaded with hydrogen. The S-parameter S_{Pd} and the mean positron diffusion length $L_{+,Pd}$ for Pd layer obtained from fitting of the $S(E)$ curves are plotted in Fig. 12b as a function of hydrogen concentration in the sample. Hydrogen charging of the epitaxial film causes a monotonic increase of S_{Pd} accompanied by a decrease of $L_{+,Pd}$. The behaviour of the S-parameter and the positron diffusion length in the epitaxial film is in this respect similar to that in the polycrystalline film testifying a hydrogen-induced plastic deformation which introduces new defects into the film. However, contrary to the polycrystalline film the epitaxial film contains a substantially higher concentration of defects already in the virgin state.

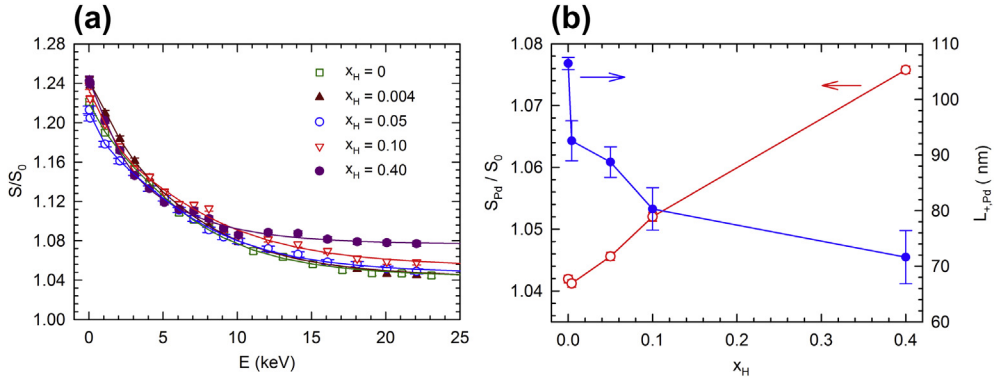

Fig. 11 – (a) $S(E)$ curves for a polycrystalline Pd film charged with hydrogen. The solid lines show the model curves calculated by the VEPFIT software; (b) The S-parameter S_{Pd} and mean positron diffusion length $L_{+,Pd}$ obtained from fitting of the $S(E)$ curves plotted as a function of hydrogen concentration x_H.

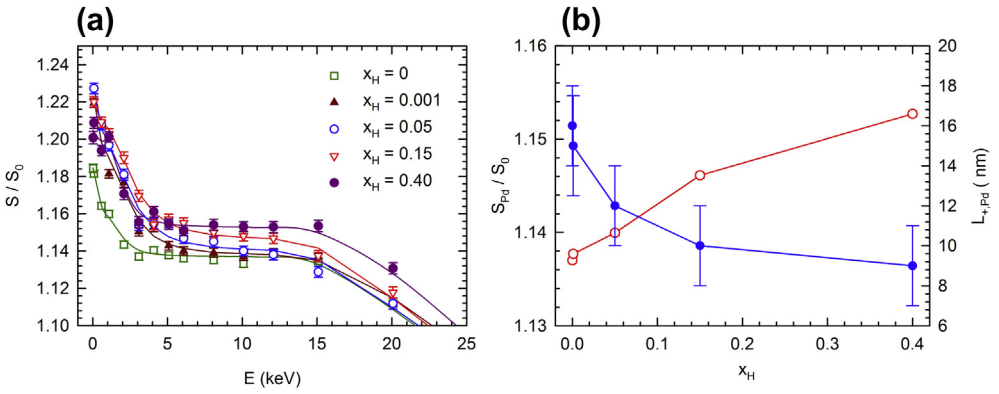

Fig. 12 – (a) $S(E)$ curves for an epitaxial Pd film charged with hydrogen. The solid lines show the model curves calculated by the VEPFIT software; (b) S-parameter S_{Pd} and mean positron diffusion length $L_{+,Pd}$ obtained from fitting of the $S(E)$ curves plotted as a function of hydrogen concentration x_H.

Note that all films studied exhibit an increase of the surface S-parameter S_{surf} with increasing hydrogen concentration, see Figs. 10(a), 11(a), 12(a), indicating that the surface roughness increases and some open-volume defects are introduced into the near surface region during electrochemical hydrogen charging.

4. Conclusions

Nanocrystalline (grain size ~ 50 nm), polycrystalline (grain size ~ 2.5 μm) and epitaxial Pd films were prepared and electrochemically charged with hydrogen. As-prepared nanocrystalline films suffer from compressive bi-axial in-plane stresses leading to an out-of-plane lattice parameter higher than in a perfect bulk Pd crystal. Contrary to this, polycrystalline and epitaxial Pd films exhibit in-plane tensile stress caused by a different thermal expansion coefficient of Pd and sapphire substrate and leading to the out-of-plane lattice parameter lower than in bulk Pd crystal. Defect studies revealed that an epitaxial film contains a very high density of dislocations. Nanocrystalline films exhibit a significant volume fraction of grain boundaries containing vacancy-like misfit defects. The lowest concentration of defects was found in the polycrystalline film.

Hydrogen introduced into the nanocrystalline film occupies firstly grain boundaries and fills vacancy-like misfit defects there. Hydrogen-induced plastic deformation takes place in all Pd films studied and introduces new defects into the films leading to an increase of the S-parameter accompanied by a decrease of positron diffusion length.

Above a certain critical hydrogen concentration buckling of the film can be initiated. It was found that this critical hydrogen concentration is influenced by the film microstructure. In the nanocrystalline film buckling occurs at hydrogen concentrations $x_H > 0.05$, while in the polycrystalline film annealed at 800 °C the binding of Pd atoms with the sapphire substrate was improved and the start of buckling was shifted to higher hydrogen concentrations $x_H > 0.4$. The epitaxial film deposited at elevated temperature exhibits the best binding to the sapphire substrate and no buckling of this film has been observed.

Acknowledgement

Financial support from the Ministry of Education, Youths and Sports of the Czech Republic (projects LH12173 and MEB101102), Deutscher Akademischer Austauschdienst DAAD (project 50755628), and availability of beamtime at the DESY, Hamburg, is highly acknowledged. AP, SW and HU also like to acknowledge the financial support by the Deutsche Forschungsgemeinschaft via PU131/9-1, PU131/10-1 and PU131/7-2.

REFERENCES

[1] Laudahn U, Pundt A, Bicker M, Hülsen U, Geyer U, Wagner T, et al. Hydrogen induced stresses in Nb-single-layers. J Alloys Comp 1999;293:490–4.
[2] Pundt A, Getzlaff M, Bode M, Kirchheim R, Wiesendanger R. Nano scale surface modifications during hydrogen absorption in Gd thin films. Phys Rev B 2000;61:9964.
[3] Pundt A, Nikitin E, Pekarski P, Kirchheim R. Adhesion energy between metal films and polymers obtained by studying buckling induced by hydrogen. Acta Mater 2004;52:1579–87.
[4] Yu Y, Kim C, Sanday SC. Buckle formation in vacuum-deposited thin films. Thin Solid Films 1991;196:229–33.
[5] Pundt A, Pekarski P. Buckling of thin niobium-films on polycarbonate substrates upon hydrogen loading. Scripta Mater 2003;48:419–23.
[6] Pundt A, Kirchheim R. Hydrogen in metals: microstructural aspects. Annu Rev Mater Res 2006;36:555–608.
[7] Weissmüller J, Lemier C. On the size dependence of the critical point of nanoscale interstitial solid solutions. Philos Magn Lett 2000;80:411–8.
[8] Wagner S, Pundt A. Mechanical stress impact on thin Pd1-xFex -films thermodynamic properties. Appl Phys Lett 2008;92:051914.
[9] Čížek J, Procházka I, Daniš S, Melikhova O, Vlach M, Žaludová N, et al. Positron annihilation study of open-volume- and dislocation-type defects occurring in nanocrystalline and epitaxial Nb–H-thin films. J Alloys Comp 2007;446–447:484–8.

[10] Flanagan TB, Oates WA. The palladium-hydrogen system. Annu Rev Mater Sci 1991;21:269–304.
[11] Pick M, Davenport JW, Strongin M, Dienes GJ. Enhancement of hydrogen uptake rates for Nb and Ta by thin surface overlayers. Phys Rev Lett 1979;43:286–9.
[12] Kircheim R. Hydrogen solubility and diffusivity in defective and amorphous metals. Prog Mater Sci 1988;32:261–325.
[13] Čížek J, Žaludová N, Vlach M, Daniš S, Kuriplach J, Procházka I, et al. Defect studies of ZnO single crystals electrochemically doped with hydrogen. Appl Phys 2008;103:053508.
[14] Lundström I, Shivaraman S, Svensson C, Lundkvist L. A hydrogen-sensitive MOS field-effect transistor. Appl Phys Lett 1975;26:55–7.
[15] Schultz PJ, Lynn KG. Interaction of positron beams with surfaces, thin films, and interfaces. Rev Mod Phys 1988;60:701–79.
[16] Anwand W, Brauer G, Butterling M, Kissenger H-R, Wagner A. Design and construction of a slow positron beam for solid and surface investigations. Defect and Diffusion Forum 2012;331:25–40.
[17] van Veen A, Schut H, Clement M, de Nijs JMM, Kruseman A, Ijpma MR. VEPFIT applied to depth profiling problems. Appl Surf Sci 1995;85:216–24.
[18] Čížek J, Procházka I, Brauer G, Anwand W, Mücklich A, Kirchheim R, et al. Defect studies of hydrogen-loaded thin Nb films. Appl Surf Sci 2006;252:3237–44.
[19] Elomari S, Boukhili R, Lloyd DJ. Thermal expansion studies of prestrained Al_2O_3/Al metal matrix composite. Acta Mater 1996;44:1873–82.
[20] Waterhouse N, Yates B. The interferometric measurement of the thermal expansion of silver and palladium at low temperatures. Cryogenics 1968;8:267–71.
[21] Campillo Robles JM, Ogando E, Plazaola F. Positron lifetime calculation for the elements of the periodic table. J Phys Condens Matter 2007;19:176222.
[22] Petroff PM, Logan RA, Savage A. Nonradiative recombination at dislocations in III–V compound semiconductors. Phys Rev Lett 1980;44:287–91.
[23] Nix WD. Mechanical properties of thin films. Metall Trans A 1989;20A:2217–45.
[24] Krause-Rehberg R, Leipner HS. Positron annihilation in semiconductors – defect studies. Berlin: Springer; 1999.
[25] Smedskjaer LC, Manninen M, Fluss MJ. An alternative interpretation of positron annihilation in dislocations. J Phys F Met Phys 1980;10:2237–49.
[26] Hautojärvi P, Corbel C. Positron spectroscopy of defects in metals and semiconductors. In: Dupasqier A, Mills A, editors. Proceedings of the international school of physics 'Enrico Fermi', course CXXV. Varenna: IOS Press; 1995. p. 491–532.
[27] Coupeau C, Naud JF, Cleymand F, Goudeau P, Grilhé J. Atomic force microscopy of in situ deformed nickel thin films. Thin Solid Films 1999;353:194–200.
[28] Mancher FD, San-Martin A, Pitre JM. H–Pd (hydrogen–palladium). In: Mancher FD, editor. Phase diagrams of binary hydrogen alloys. Materials Park: ASM International; 2000. p. 158–81.
[29] Mütschele T, Kirchheim R. Hydrogen as a probe for the average thickness of a grain boundary. Scripta Metall 1987;21:1101–4.